Front. Earth Sci. 2015, 9(4): 594–604
DOI 10.1007/s11707-014-0489-9

RESEARCH ARTICLE

Sensitivity study of subgrid scale ocean mixing under sea ice using a two-column ocean grid in climate model CESM

Meibing JIN (✉)[1], Jennifer HUTCHINGS[2], Yusuke KAWAGUCHI[3]

1 International Arctic Research Center, University of Alaska Fairbanks, AK 99775, USA
2 College of Earth, Ocean and Atmospheric Sciences, Oregon State University, OR 97331, USA
3 Japan Agency for Marine-Earth Science and Technology, Yokosuka 237-0061, Japan

Abstract Brine drainage from sea ice formation plays a critical role in ocean mixing and seasonal variations of halocline in polar oceans. The horizontal scale of brine drainage and its induced convection is much smaller than a climate model grid and a model tends to produce false ocean mixing when brine drainage is averaged over a grid cell. A two-column ocean grid (TCOG) scheme was implemented in the Community Earth System Model (CESM) using coupled sea ice-ocean model setting to explicitly solve the different vertical mixing in the two sub-columns of one model grid with and without brine rejection. The fraction of grid with brine rejection was tested to be equal to the lead fraction or a small constant number in a series of sensitivity model runs forced by the same atmospheric data from 1978 to 2009. The model results were compared to observations from 29 ice tethered profilers (ITP) in the Arctic Ocean Basin from 2004 to 2009. Compared with the control run using a regular ocean grid, the TCOG simulations showed consistent reduction of model errors in salinity and mixed layer depth (MLD). The model using a small constant fraction grid for brine rejection was found to produce the best model comparison with observations, indicating that the horizontal scale of the brine drainage is very small compared to the sea ice cover and even smaller than the lead fraction. Comparable to models using brine rejection parameterization schemes, TCOG achieved more improvements in salinity but similar in MLD.

Keywords climate model, sea ice, mixed-layer depth, ocean mixing, brine drainage

1 Introduction

Brine drainage from growing sea ice is a major driver for the vertical mixing and plays an important role in modulating buoyancy forcing and tracer transport in the polar oceans during the winter months. The brine rejection rates under different sea ice thickness or lead (gaps between sea ice blocks) are highly variable and the spatial scales are not resolved by climate model grid (usually much greater than 1 km). Heat loss through leads can be up to $300\,W\cdot m^{-2}$, 15 times that from the surrounding ice (Morison, 1993), and the majority of sea ice growth in the Central Arctic Ocean occurs in leads (Wettlaufer et al., 1997). Arctic leads, especially during winter, are in general close to a state of free convection and strong convection driven by the extruded brine in a refreezing lead drives vigorous mixing in the mixed layer immediately below, irrespective of the advective velocity of ice (Kantha, 1995). The numerical experiments (Matsumura and Hasumi, 2008) showed that brine plume from leads sinks until it reaches higher density (at or a little over mixed layer depth) and spreads horizontally. The ocean mixing occurs in a similar horizontal size and shape as the lead and needs subgrid-scale parameterization to correctly simulate in climate models. The brine rejection under flat sea ice cover is also not uniform. After ice reaches certain critical thickness, the brine drainage process is controlled by major brine channels (Figs. 1(a) and 1(b) from Lake and Lewis, 1970). The brine plume dropping out of major brine channels sinks with little horizontal mixing as shown by dye in the laboratory (Fig. 1(c) by Wakatsuchi and Ono, 1983). 'Brinicile' ice finger filmed in the Antarctic Ocean (Fig. 1(d)) is a visual example of how a brine plume sinks with little horizontal mixing before stopped by ocean bottom (the refreezing on the ocean bottom is due to the decreased salinity and freezing point as the brine is diluted).

Received August 21, 2014; accepted October 21, 2014

E-mail: mjin@alaska.edu

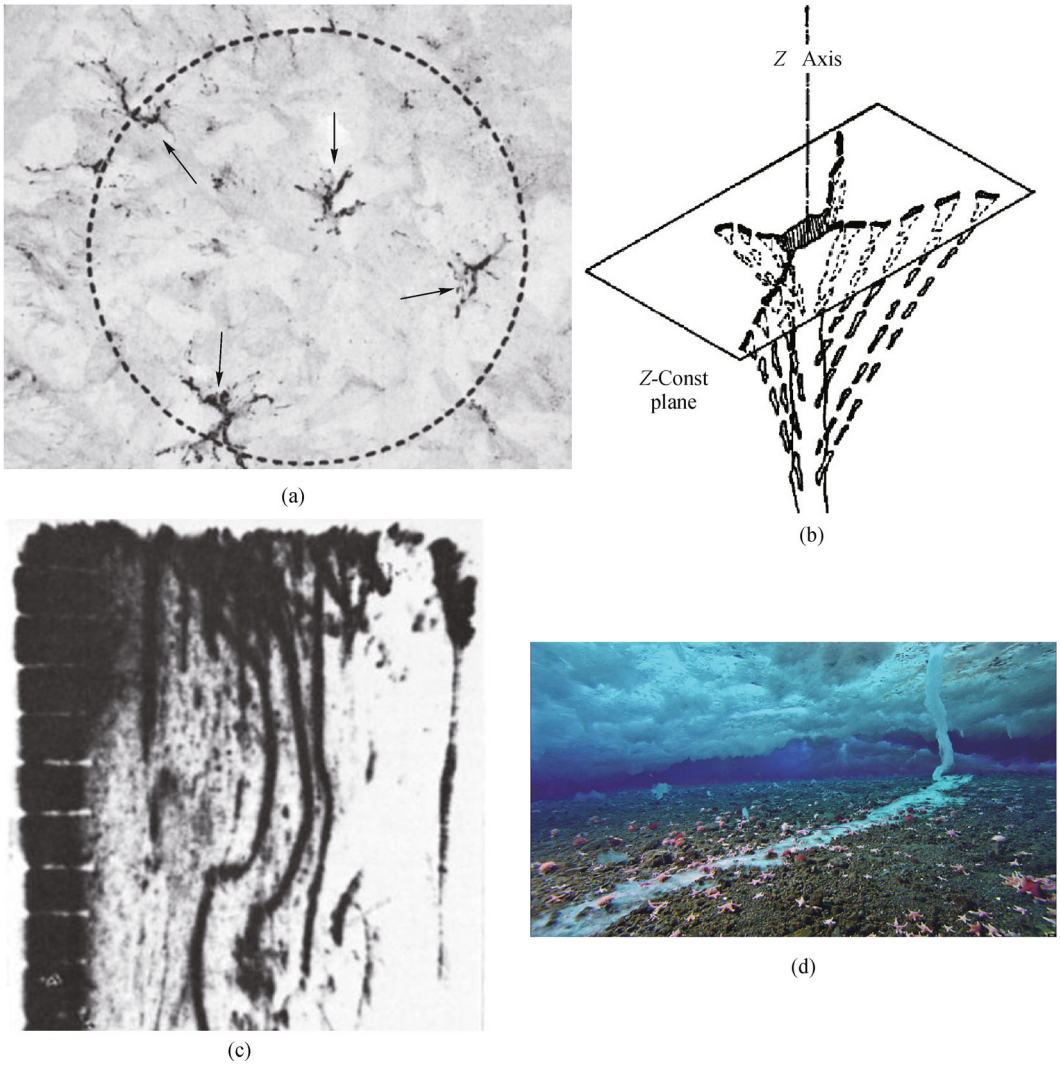

Fig. 1 (a) Horizontal section of sea ice with major brine channels shown by arrows; (b) Schematic drawing of a brine drainage channel and its feed arms from Lake and Lewis (1970); (c) Side view of sinking brine plume dye in water (the scales in the left are 1 cm interval) from Wakatsuchi and Ono (1983); (d) 'Brinicle' ice finger in Antarctic by BBC nature news (http://www.bbc.co.uk/nature/15835017).

Climate model grid is much larger than the drainage channels or most of leads in the real ocean and the grid cannot match the brine plume due to its fixed shape and position. The brine drainage is usually averaged over a model grid and will fill the entire upper mixed layer water (Fig. 2(a)), in contrast to the actual brine plume sinking process that brings most of the brine to the bottom of mixed layer with much smaller contribution to the surface water, especially those not directly under the drainage channel (Fig. 2(b)). Using homogeneous brine rejection rate in one grid cell results in model errors biased toward higher sea surface salinity and deeper ocean mixed layer depth (MLD) compared to observations. Parameterizations of this type of subgrid scale ocean mixing have been studied in Duffy et al. (1999), Nguyen et al. (2009) and Jin et al. (2012) by artificially applying the brine rejection from ice formation directly into deeper layers in the upper mixed layer. The parameterization can significantly reduce model biases.

The purpose of this study is to use a two-column ocean grid (TCOG) in an ocean model to explicitly study the subgrid scale ocean mixing process and assess the resulted model improvements compared to the previous studies using parameterization schemes. By assuming that brine rejection only occur in a small portion of a model grid during a given time period (e.g., one model time step at one hour), the two ocean columns in TCOG represent one portion of grid with brine drainage and the other without. Detailed model setting and results are discussed in the following sections.

2 Model setting

The model experiments are conducted using the ice and ocean components of the widely used Community Earth System Model (CESM, http://www.cesm.ucar.edu/models/):

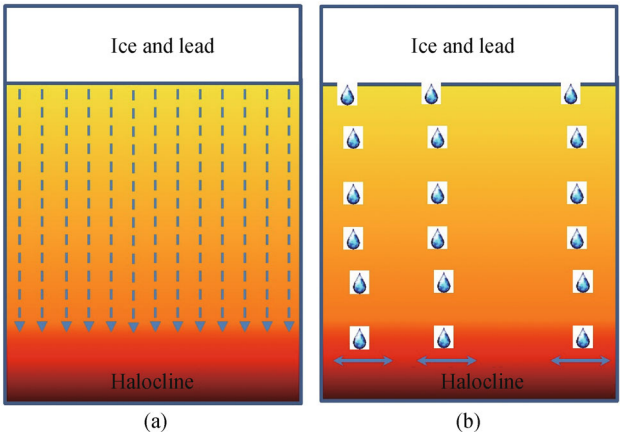

Fig. 2 Schematic plot of brine drainage distribution in one ocean model grid (a) in climate models, (b) in real ocean. The density is homogenous in the upper mixed layer but jumps in the halocline due to increase salinity in the Arctic Ocean.

Parallel Ocean Program (POP, Danabasoglu et al., 2012) and the Los Alamos sea ice model (CICE, Hunke et al., 2013), that communicate through a coupler. POP solves the primitive equations with hydrostatic and Boussinesq approximations with an implicit free-surface formulation for barotropic equation. CICE solves thermodynamics in the vertical snow and ice layers and dynamics in the horizontal space including ice advection and ridging. There are five types of predictive state variables (Bitz et al., 2001) in CICE: ice concentration, ice volume, snow volume, energy of ice melting in each ice thickness category (ITC) i and mean ice velocity in a grid cell (g_i,V_i,V_i^s,E_i,u). Currently, The model setting includes five ITCs (i = 1 to 5). The sea ice concentration and lead fraction in a grid cell are calculated as $A_{ice} = \sum_1^5 g_i$ and $g_0 = 1 - \sum_1^5 g_i$. Ice thickness is diagnosed from ice volume and ice concentration.

We used the default parameter setting for POP and CICE in the CESM 1.2 release except setting the background mixing coefficient to 0.01 cm^2/s in the Arctic — the optimal value recommended by Zhang and Steele et al. (2007). The POP-CICE runs on a global GX1 grid: 'nominal' 1-degree horizontal resolution with x, y dimensions at 320 × 384 and a displaced North Pole in Greenland. The horizontal grid in the Arctic is between 30 and 50 km. The POP has 60 vertical layers and the resolution is 10 m in the upper 150 m, and increases to a maximum of 250 m in deep oceans (Danabasoglu et al., 2012).

The model is forced by six-hourly NCEP reanalysis data (Large and Yeager, 2009) for 32 years (1978–2009). The sea ice and ocean starts from rest; initial ocean temperature and salinity are from the Polar Science Center Hydrographic Climatology (PHC; Steele et al., 2001) for January. Model-data comparisons are focused on the years 2005 to 2009. Since comparisons are focused on the upper 150 m, a 27 year spin up (1978–2004) is found to be adequate for this study (even the model starts from 1990, the model comparison is almost the same).

Heat and salt fluxes received by ocean model are calculated from CICE for each ITC, and from the atmospheric driver for the open water portion. The fluxes are averaged over each ITC and open water ppotion into one flux in single column grid (Control case). The TCOG scheme uses two sub-grid columns implemented in each POP grid: one column with brine rejection (fraction =p_0<100%) and the other column (fraction = $1-p_0$) without brine rejection. Here, p_0 is the only parameter in the TCOG scheme and will be investigated using sensitivity studies. The following variables and processes are computed separately in each column (applied in all depth levels): 1) VDCS, VDCT and VVC, the vertical diffusivity coefficients for salinity (S) and temperature (T), and vertical viscosity coefficient for momentum. These coefficients are used in vertical diffusion terms $\frac{\partial}{\partial z}\left(VDCT\frac{\partial T}{\partial z}\right)$, $\frac{\partial}{\partial z}\left(VDCS\frac{\partial S}{\partial z}\right)$ and viscosity term $\frac{\partial}{\partial z}\left(VVC\frac{\partial \vec{u}}{\partial z}\right)$ (here, z is vertical coordinate and $\vec{u}$ is horizontal velocity). In CESM, these coefficients are calculated in k-profile parameterization (KPP, Large et al., 1994) turbulence model; and 2) at the end of each time step, VDCS, VDCT, and VVC in the two columns are averaged, weighted by their fractions. After the average, the subsequent computations are the same as in the single-column ocean grid model.

A series of model experiments (Table 1) are designed to investigate the fraction p_0 in TCOG as either equal to the fraction of lead or a fixed fraction where brine rejection from sea ice is present. The control case uses the regular single column ocean model grid. In TCOG cases, except that the salt flux due to brine drainage is allocated to the fraction p_0 column, all other fluxes (including heat fluxes) to ocean model is equal to the average in both columns. The brine drainage is calculated as the sum of brine rejection from all sea ice categories and evaporation minus precipitation in leads, and these fluxes are already calculated in the current CESM. The brine rejection parameterization in scheme by Nguyen et al. (2009) and Jin et al. (2012) are implemented in CESM as comparison cases NA and JM (Table 1). Single column ocean grid is used in NA and JM scheme and the brine (Sb in unit of ppt) is vertically distributed as

$$Sb(z) = \begin{cases} Az^n & \text{if } |z| < MLD \\ 0 & \text{if } |z| < MLD \end{cases}. \quad (1)$$

Here z is depth, n is an adjustable parameter and implies the distribution power of salt with depth. Nguyen et al. (2009) recommends optimum n = 5; and Jin et al. (2012) defined n as an empirical function of lead fraction g_0. A is

Table 1 Model cases in the sensitivity study and their corresponding modeled northern hemisphere sea ice volume averaged over 2005 to 2009

Case name	Control	LE	F2	F3	F4	F5	F6	F7	NA	JM
Fraction p_0		Lead fraction g_0	10^{-2}	10^{-3}	10^{-4}	10^{-5}	10^{-6}	10^{-7}	Nguyen et al. (2009)	Jin et al. (2012)
Ice volume /(10^{12}m^3)	15.87	15.92	15.93	15.96	15.99	16.01	16.04	16.14	15.95	15.93

determined by the total brine rejection (Sb_{total} in unit of ppt), the distribution power n, and the mixed layer depth:

$$A = \frac{(n+1)Sb_{total}}{MLD^{(n+1)}}. \quad (2)$$

3 Results and discussion

3.1 Effects of TCOG on sea ice extent and thickness

The simulated monthly mean northern-hemisphere sea ice extent of the Control case captured the large scale seasonal and interannual variations in sea ice coverage, as compared with the National Snow and Ice Data Center (NSIDC) data (Fetterer et al., 2002, Fig. 3(a)). The effects of TCOG on sea ice extents are very small and the results are too close to the Control case to be shown in Fig. 3(a).

Sea ice thickness and lead fraction were derived from three moored upward looking sonar (ULS) in the Canadian Basin (locations shown in Fig. 3(b)) in 2004–2007 for model validation. The observed ice draft was converted to ice thickness using a simple ratio of 1.1, and the lead fraction is the percentage of measurements with ice thickness < 0.2 m. The modeled thickness and lead of all cases were very close (Figs. 3(c) and 3(d), only Control and LE cases are shown here) and the model results matched well with thickness observations in most time and locations — though the model underestimated ice thickness and overestimated lead fraction for station B and C in 2004 and 2005. The modeled ice thickness matched well with observation where the lead fraction matched well with observation, which indicates that correctly simulating lead fraction is critical for the simulation of ice thickness, because the air-sea heat exchange through lead is much higher than through sea ice and more new ice is formed in lead.

The maximum relative difference of modeled northern hemisphere sea ice volume averaged over 2005 to 2009 between all cases is 1.68% (Table 1). The sea ice volume was lower in the Control case than all cases, and there is a trend of higher ice volume with lower p_0 in the F-cases (F2 to F7 in Table 1). This is because the ocean MLD is deeper for lower p_0 F-cases as shown later, and the deeper the brine drainage induced ocean mixing can reach, the more heat content from deep water can be brought to the surface mixed layer to melt sea ice.

3.2 Effects of TCOG on ocean temperature, salinity and mixed layer depth

Ocean model results were validated with long-time series of temperature (T) and salinity (S) vertical profiles from 29 Ice Tethered Profilers (ITP, Toole et al., 2010). Most ITPs were deployed for one year or more (Table 2) and their tracks are shown in Fig. 4. The ITP data are chosen for the TCOG model validation because they have the best year round and large spatial coverage of the Arctic Ocean basins, especially in winter time when TCOG matters most during ice formation, while ship measurements were mostly conducted in summer and had limited spatial coverage. The ITP T and S data were first averaged at daily and vertically 10 m intervals and then MLD was calculated using the method of Large et al. (1997) which is the same as in the POP model: the shallowest depth where the local, interpolated buoyancy gradient matched the maximum buoyancy gradient between the surface and discrete depth within that water column. Altogether, there are 8,906 daily averaged vertical profiles, among which 5,860, 2,056 and 990 are in the region 1 (Canada Basin), 2 (Makarov Basin) and 3 (Eurasian Basin), respectively, as their tracks colored differently in Fig. 4. The model results were extracted from the same locations and day along the ITP tracks for comparison. Table 3 showed the root mean square errors (RMSE) of modeled salinity, temperature and MLD vs. ITP data and the relative improvements (RI in unit of %) of all sensitivity cases over Control cases. For salinity, all TCOG cases and NA, JM cases showed significant reduction of RMSE (or model improvements) in all regions, except case F7 in region 1. The model improvement increases from case F2 to F6, but decreases from F6 to F7. Case F6 has the highest model improvements over all other cases in all regions, which indicates the optimum parameter $p_0 = 10^{-6}$. The model improvements of case LE and F3 are similar because the average lead fraction is close to 10^{-3} in winter as shown in Fig. 3(d). The brine-induced convection might occur in less than lead fraction due to two factors: 1) observations and modeling found that the convection are stronger at the edge of lead (Kantha, 1995), which means strong convection only occurs under part of the lead; 2) the brine drainage under sea ice are only from major drainage channels, which is a small percentage of the ice cover, and also, drainage from those channels may not happen at the same time (e.g., Fig. 1(d)) which makes the fraction with brine drainage even smaller. Case

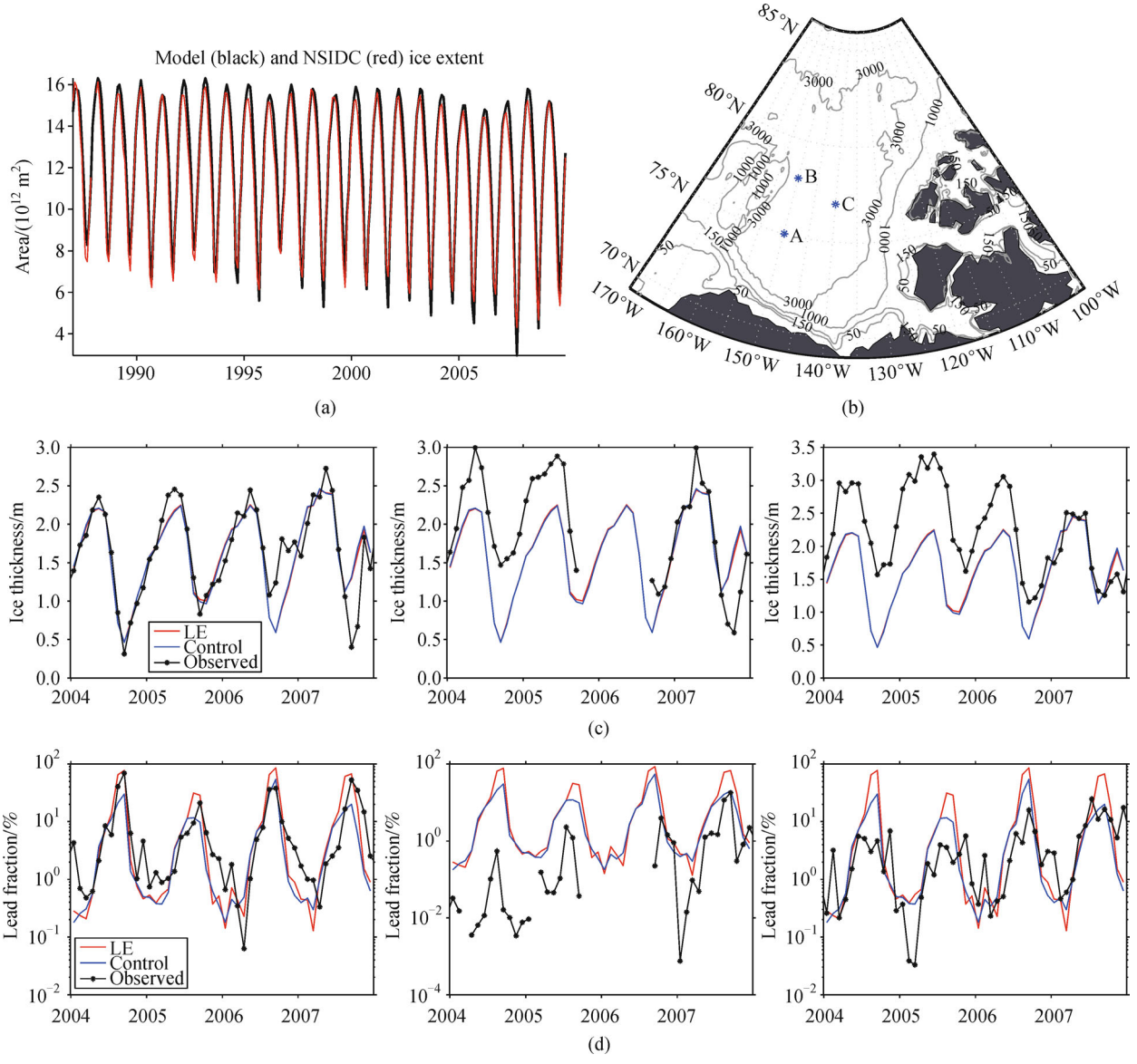

Fig. 3 (a) Comparison of the monthly modeled (Control case) and NSIDC sea ice extent in the northern hemisphere; (b) location of stations A, B and C of ice thickness measurements. Comparison of the monthly modeled (Control and LE case) and observed; (c) ice thickness (m) and (d) lead fraction (%). Stations A, B and C are from left to right in (c) and (d).

F6 achieved about 30% better model improvement than NA and JM cases, because the depth that brine drainage can sink to is more realistically computed using KPP turbulence model in TCOG case, vs. the MLD used in NA and JM cases. The model improvement for temperature is relatively small (Table 3), and F6 case has the highest improvement for all regions at 3.82%. The improvements for MLD are significant in all regions and for all cases, similar to the improvements for salinity. The NA case has the highest MLD improvement for all regions at 57.74%, slightly more than cases F4, F5 and F6.

Modeled MLD of four cases (Control, LE, F6 and NA) was compared to the ITP data in region 1 (Fig. 5), 2 (Fig. 6) and 3 (Fig. 7). The MLDs of other cases are falling between those of the Control and F6 cases in consistent with the order of their model improvement of S (Table 3) and thus not shown in Figs. 5–7. Most of the observed MLD increased in early arctic winter (Oct. to Dec.), but not in late winter (from Jan. to May) before ice melt. All modeled MLD matches well with observation in summer, but the MLD of the Control case increased faster in early winter and continued to increase in late winter to be much deeper than those of the observed and other cases. It is evident along the all ITP tracks (Figs. 5–7) that the MLD of

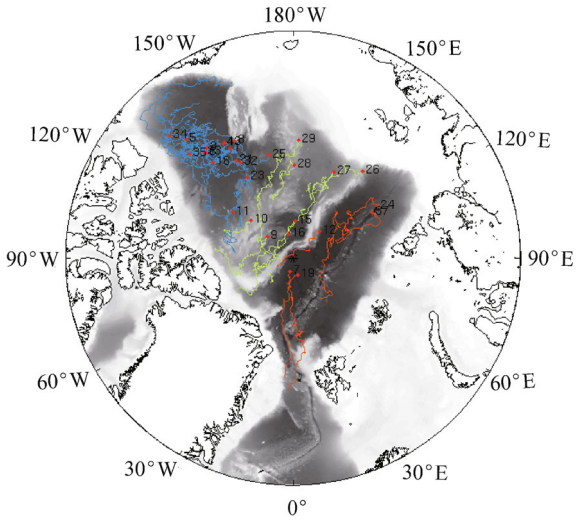

Fig. 4 Ice Tethered Profiler (ITP) tracks from 2005 to 2009. The Arctic Basin are divided into region 1 (Canada Basin), 2 (Makarov Basin) and 3 (Eurasian Basin) as the tracks in them are colored in purple, green and red.

the LE, F6 and NA cases were significantly improved over Control case, while the MLD of F6 and NA cases were similar and achieved better improvements over that of the LE case. The MLD of F6 case matched better with observations in region 3 than in region 2 and 1 (Figs. 5–7), consistent with the ranking of the relative model improvements of S among those three regions (Table 3).

Simulated pan-Arctic monthly mean MLDs of the Control and F6 cases in March of year 2009 were compared with MLD calculated from PHC monthly climatology of T and S (Fig. 8). The MLD in the Control case was up to around 80 m in the Arctic Basin area, vs. observed MLD of up to 40 m, suggesting that there was excessive vertical mixing in the Control case over the entire Arctic Basins. The F6 case significantly reduced MLD error in the Arctic Basin, with the most reduction in the Canada Basin: a 30 m to 40 m reduction of MLD (Fig. 8(d)).

4 Discussion and conclusion

The accuracies of climate model predictions are compromised by many unresolved subgrid scale physics, such as turbulence, small scale topographic features and sea ice cover, etc. In this study, the subgrid scale ocean mixing under heterogeneous sea ice cover was investigated with a TCOG scheme. Sensitivity study of the TCOG cases showed consistent improvement of modeled S and MLD indicating improved simulation of ocean mixing that is comparable to (in terms of simulated MLD) and better than (in terms of simulated salinity) those of the parameterization in NA and JM cases.

The warm subsurface Pacific Water in 30 m to 60 m depth range and intermediate Atlantic Water under 150 m in the Arctic Ocean basins are isolated from melting sea ice cover by the strong upper ocean halocline. Ocean mixing

Table 2 List of ITP data. The ITP number is the number counted in the order the ITP was implemented in the Arctic Ocean. The missing numbers are those with few or no data due to instrument failure. The region is defined in Fig. 4. The starting and ending time of ITPs are in the format of 'year. month.day'

ITP number	Region	Starting time	Ending time	ITP number	Region	Starting time	Ending time
1	1	2005.08.16	2007.01.06	19	3	2008.04.08	2008.11.21
3	1	2005.08.24	2006.09.08	21	1	2008.08.04	2009.09.23
4	1	2006.09.03	2007.08.17	23	1	2008.08.05	2010.07.06
5	1	2006.09.08	2007.09.06	24	3	2008.10.03	2009.09.25
6	1	2006.09.05	2008.06.23	25	1	2008.09.22	2009.07.07
7	3	2007.04.28	2007.10.24	26	2	2008.09.11	2009.03.11
8	1	2007.08.13	2009.03.23	27	2	2008.09.10	2009.01.20
9	2	2007.09.12	2008.10.03	28	2	2008.09.01	2008.12.18
10	2	2007.09.10	2008.05.15	29	2	2008.08.31	2010.09.15
11	1	2007.09.09	2009.09.03	32	1	2009.10.04	2010.01.13
12	3	2007.09.15	2007.12.23	33	1	2009.10.07	2011.01.24
13	1	2007.08.14	2008.07.16	34	1	2009.10.11	2010.11.26
15	2	2007.09.11	2008.10.05	35	1	2009.10.09	2010.03.30
16	2	2007.09.03	2008.01.01	37	3	2009.08.30	2010.12.24

Table 3 Root mean square errors (RMSE) of modeled S, T in the upper 150 m and MLD as compared with the ITP data. Relative improvements (%) over the Control case are calculated as $\mathrm{RI} = \frac{\mathrm{RMSE}_{\mathrm{Control}} - \mathrm{RMSE}_{\mathrm{Case}}}{\mathrm{RMSE}_{\mathrm{Control}}} \times 100\%$. The numbers in bold font denote the best performer of all cases in each line

Variable region	Case name	Control	LE	F2	F3	F4	F5	F6	F7	NA	JM
S 1	RMSE	1.18	1.04	1.09	1.04	1.02	0.98	0.96	1.21	1.04	1.04
	RI		11.6	7.9	11.7	13.8	16.3	18.6	−2.9	11.8	11.7
S 2	RMSE	1.12	0.96	1.01	0.95	0.93	0.90	0.89	1.06	0.94	0.94
	RI		14.4	10.2	14.8	17.1	19.8	20.6	5.8	16.4	15.8
S 3	RMSE	1.10	0.95	1.00	0.94	0.91	0.87	0.84	0.97	0.89	0.89
	RI		13.8	9.1	14.1	17.5	21.2	23.4	11.4	19.2	18.6
S All 3	RMSE	1.15	1.00	1.05	1.00	0.97	0.94	0.92	1.13	0.99	0.99
	RI		12.7	8.7	12.9	15.3	18.1	19.9	1.8	14.3	14.0
T 1	RMSE	0.46	0.41	0.43	0.41	0.40	0.39	0.40	0.46	0.39	0.39
	RI		9.89	6.20	10.82	12.63	14.23	11.97	−1.27	14.99	14.74
T 2	RMSE	0.25	0.29	0.26	0.30	0.31	0.32	0.28	0.21	0.37	0.36
	RI		−17.91	−6.93	−20.30	−27.29	−29.87	−13.08	13.99	−50.76	−43.86
T 3	RMSE	0.44	0.48	0.46	0.48	0.49	0.49	0.48	0.49	0.51	0.50
	RI		−7.69	-4.68	−7.87	−9.55	−10.61	−8.10	−11.45	−14.72	−13.70
T All 3	RMSE	0.40	0.39	0.39	0.39	0.39	0.39	0.38	0.40	0.41	0.40
	RI		1.75	1.86	1.90	1.53	1.90	3.82	−0.61	−1.98	−0.76
MLD 1	RMSE	30.77	8.09	22.43	17.04	13.55	12.44	13.90	16.79	12.28	13.01
	RI		41.19	27.09	44.61	55.97	59.55	54.81	45.42	60.10	57.71
MLD 2	RMSE	24.81	15.14	18.10	14.13	11.42	10.73	11.10	12.53	10.93	11.78
	RI		8.97	27.06	43.04	53.95	56.73	55.26	49.48	55.96	52.51
MLD 3	RMSE	21.55	3.99	6.12	12.84	11.43	10.92	10.93	11.58	10.72	11.09
	RI		5.05	5.17	40.43	46.97	49.33	49.25	46.24	50.23	48.54
MLD	RMSE	27.53	6.57	0.15	15.51	12.60	11.71	12.62	14.72	11.64	12.34
All 3	RI		9.81	6.82	43.66	54.25	57.47	54.17	46.54	57.74	55.18

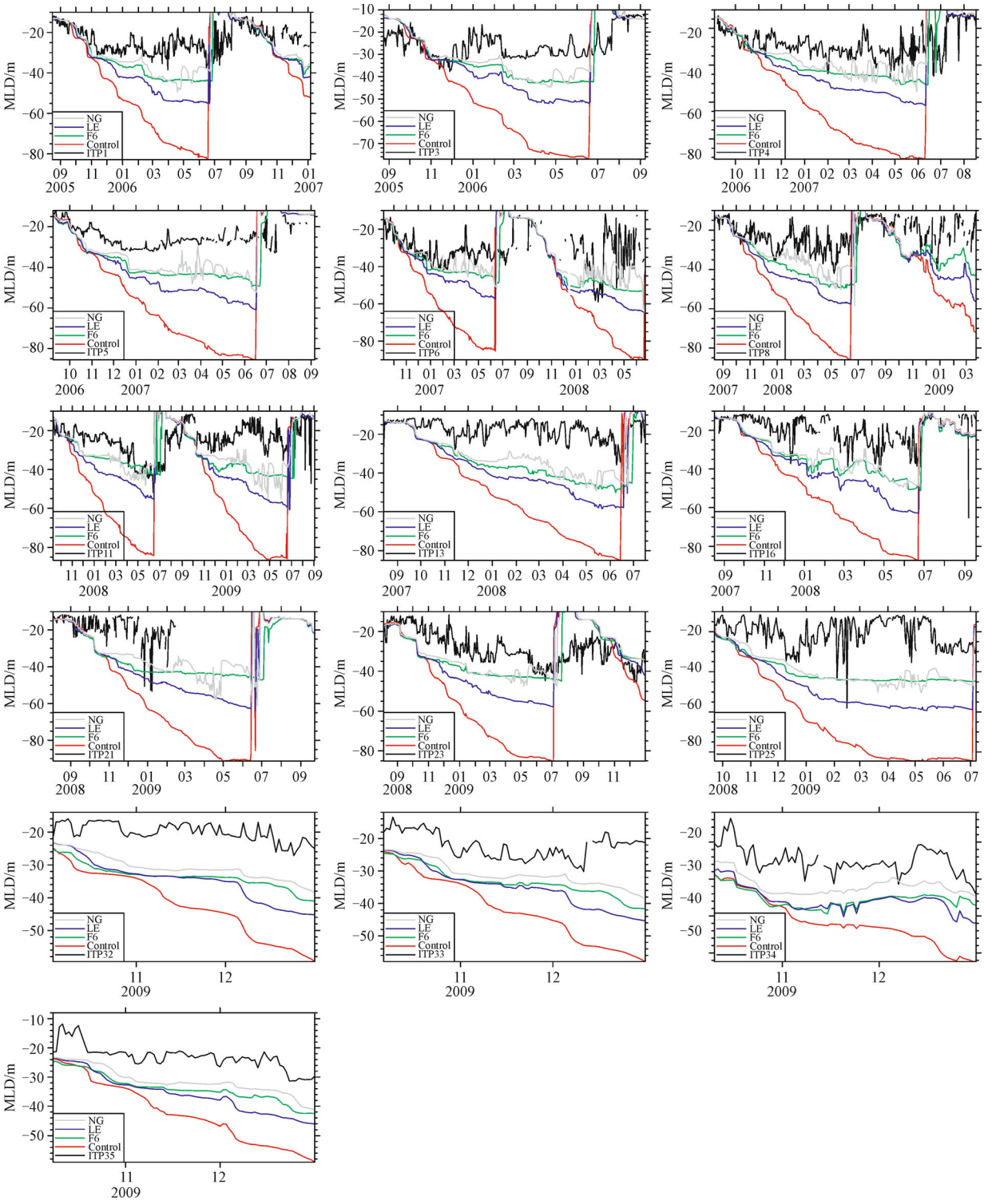

Fig. 5 Comparison of MLD from model simulation and ITP data along ITP track in region 1.

under sea ice is a critical process for the seasonal variations of the halocline in the Arctic Ocean which can significantly influence the simulated temperature and salinity in the water column and the sea ice area. This kind of influences was shown by the lower modeled sea ice volumes (Table 1) in cases with deeper ocean MLD (such as Control case vs.

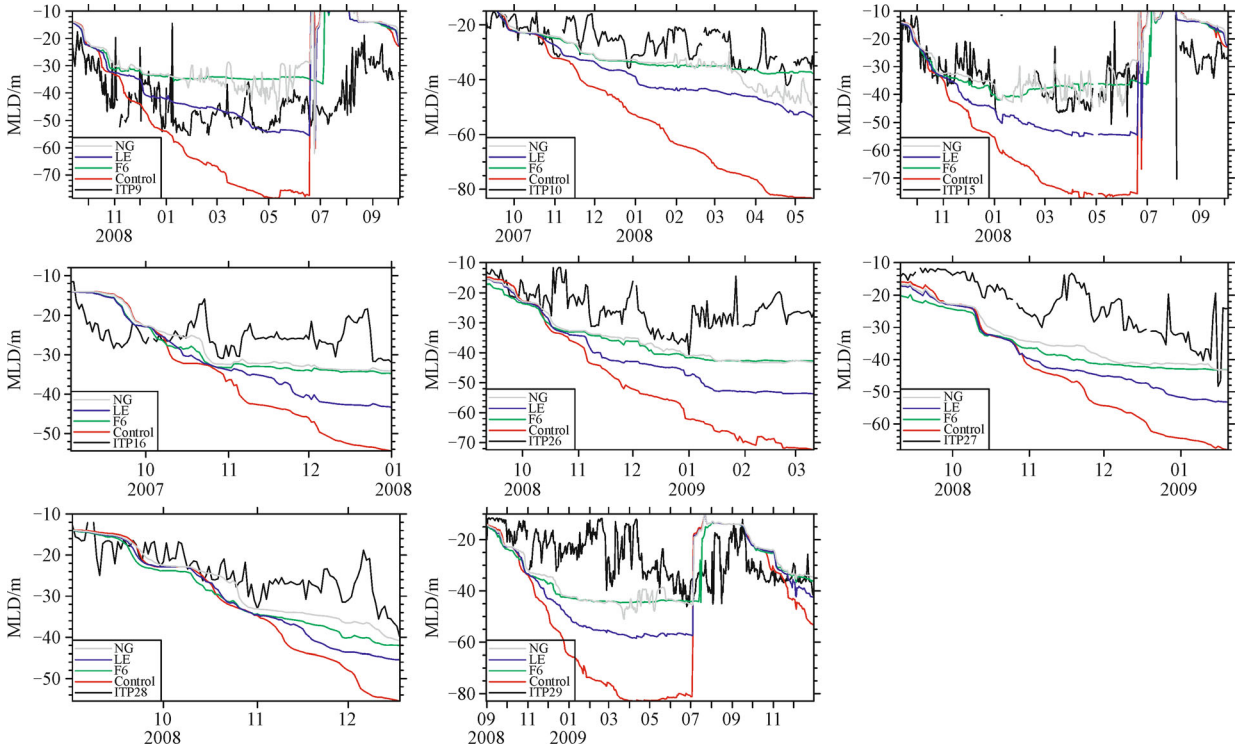

Fig. 6 The same as Fig. 5 but in region 2.

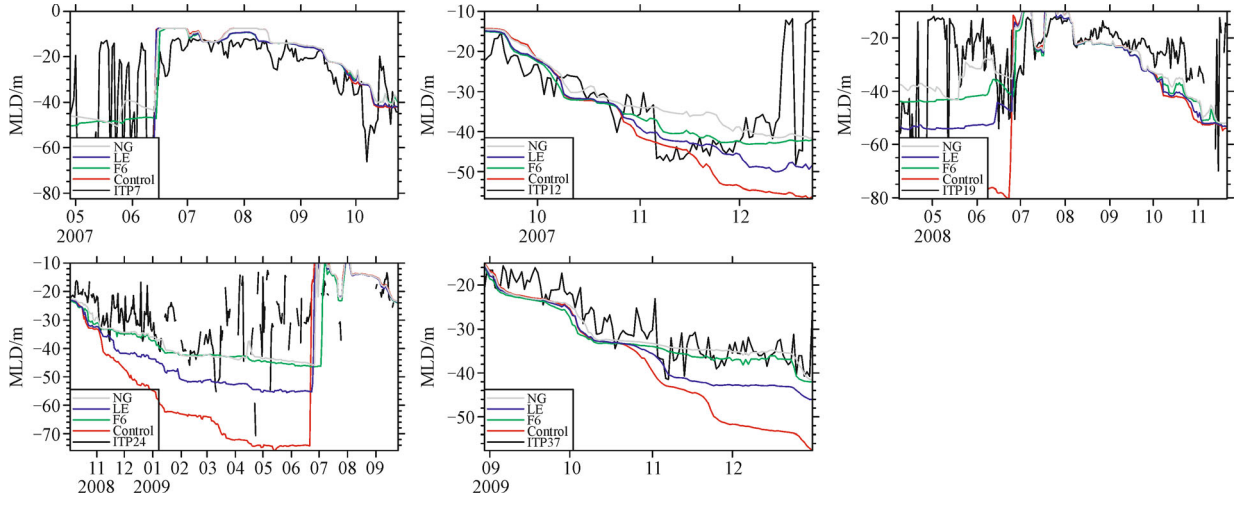

Fig. 7 The same as Fig. 5 but in region 3.

F6 case in Figs. 5–7). The TCOG scheme is beneficial in improving the simulated MLD and vertical profiles of the upper ocean salinity, and therefore the sea ice volume as well, although the magnitude of the resulted differences in the north hemisphere sea ice volume are small (Table 1).

The optimum case F6 indicates that brine drainage and the resulted ocean convection in the Arctic Ocean is confined to a very small fraction (around 10^{-6}) under ice and lead. This number is related to the lead fraction (although the optimum number is smaller than the lead fraction) and the fraction of major drainage channel in sea ice and how often the drainage of brine occurs. Since this

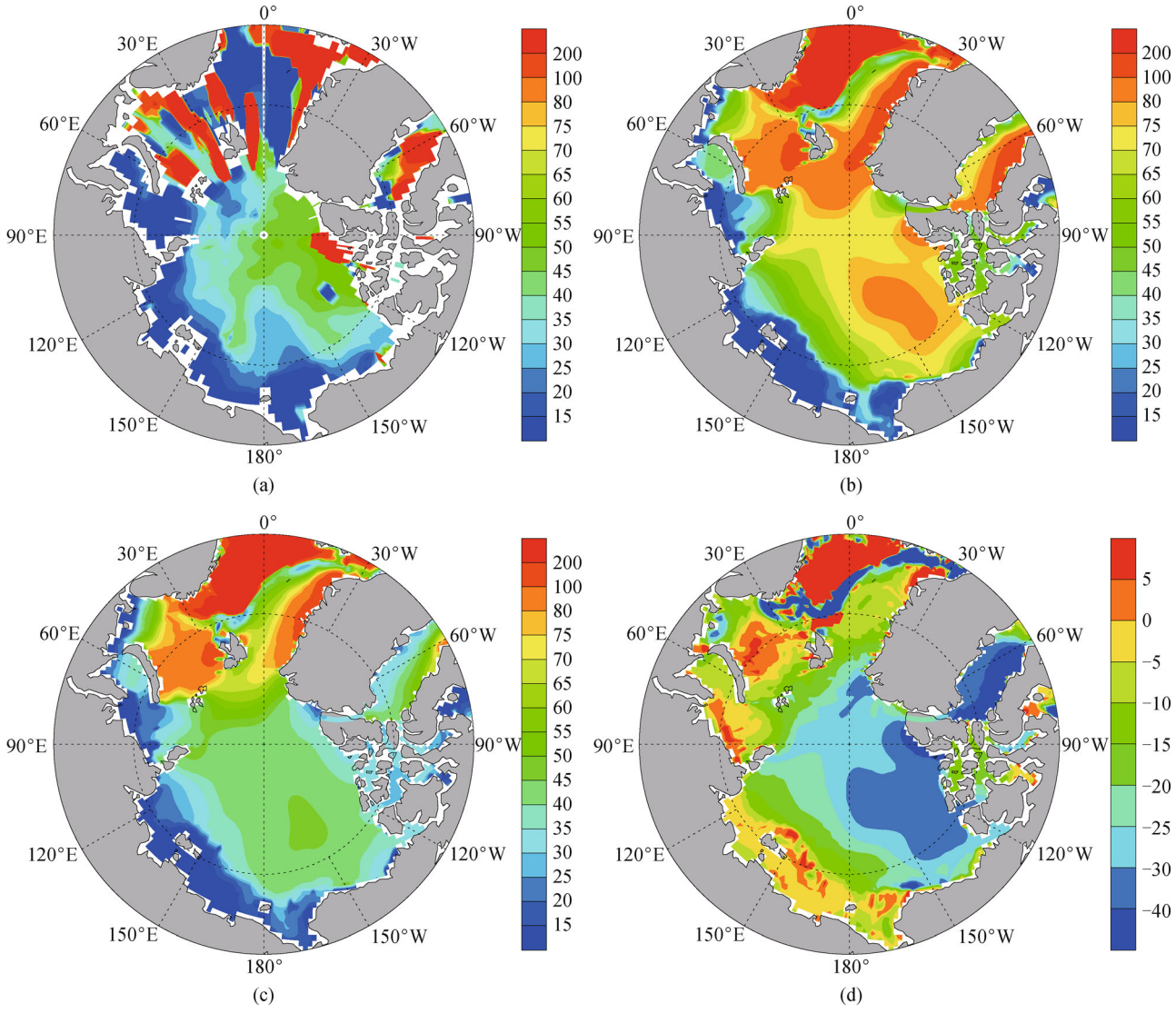

Fig. 8 March mean MLD of (a) climatology observation from PHC3.0, (b) Control case, (c) F6 case, and (d) F6 case minus Control case of year 2009.

fraction is not a direct prognostic variable in the current sea ice models, our knowledge on this spatial scale demands more in situ measurements in the future.

Acknowledgements This work is funded by the NSF Climate Process Team (CPT) project ARC-0968676. We appreciate the computational support by Arctic Region Supercomputer Center (ARSC/UAF). The ULS and ITP data were collected and made available by the Beaufort Gyre Exploration Program and ITP program based at the Woods Hole Oceanographic Institution.

References

Bitz C M, Holland M M, Weaver A J, Eby M (2001). Simulating the ice-thickness distribution in a coupled climate model. J Geophys Res, 106(C2): 2441–2463

Danabasoglu G, Bates S, Briegleb B P, Jayne S R, Jochum M, Large W G, Peacock S, Yeager S G (2012). The CCSM4 ocean component. J Clim, 25(5): 1361–1389

Duffy P, Eby M, Weaver A (1999). Effects of sinking of salt rejected during formation of sea ice on results of an ocean-atmosphere-sea ice climate model. Geophysical Research Letter, 26(12), 1739–1742

Fetterer F, Knowles K, Meier K, Savoie M (2002). Updated 2009. Sea Ice Index [ice extent]. Boulder: National Snow and Ice Data Center.

Hunke E C, Lipscomb W H, Turner A K, Jeffery N, Elliott S (2013). CICE: The Los Alamos Sea Ice Model Documentation and Software User's Manual Version 5.0 LA-CC-06–012, Los Alamos National Laboratory, USA

Jin M, Hutchings J, Kawaguchi Y, Kikuchi T (2012). Ocean mixing with lead-dependent subgrid scale brine rejection parameterization in climate model. J Ocean Univ China, 11(4): 473–480

Kantha L H (1995). A numerical model of Arctic leads. J Geophys Res,

100(C3): 4653–4672

Lake R A, Lewis E L (1970). Salt rejection by sea ice during growth. J Geophys Res, 75(3): 583–597

Large W, Danabasoglu G, Doney S, McWilliams J (1997). Sensitivity to surface forcing and boundary layer mixing in the NCAR CSM ocean model: annual-mean climatology. J Phys Oceanogr, 27(11): 2418–2447

Large W G, McWilliams J C, Doney S C (1994). Oceanic vertical mixing: a review and a model with a vertical K-profile boundary layer parameterization. Rev Geophys, 32(4): 363–403

Large W G, Yeager S G (2009). The global climatology of an interannually varying air-sea flux data set. Clim Dyn, 33(2-3): 341–364

Matsumura Y, Hasumi H (2008). Brine-driven eddies under sea ice leads and their impact on the Arctic Ocean mixed layer. Journal of Physical Oceanography, 38: 146–163

Morison J H (1993). The lead experiment. Eos Trans AGU, 74(35): 393–397

Nguyen A T, Menemenlis D, Kwok R (2009). Improved modeling of the Arctic halocline with a subgrid-scale brine rejection parameterization. J Geophys Res, 114(C11): C11014

Steele M, Morley R, Ermold W (2001). PHC: a global ocean hydrography with a high quality Arctic Ocean. J Clim, 14(9): 2079–2087

Toole J M, Timmermans M L, Perovich D K, Krishfield R A, Proshutinsky A, Richter-Menge J A (2010). Influences of the ocean surface mixed layer and thermohaline stratification on Arctic Sea ice in the central Canada Basin. J Geophys Res, 115(C10): C10018

Wakatsuchi M, Ono N (1983). Measurements of salinity and volume of brine excluded from growing sea ice. J Geophys Res, 88(C5): 2943–2951

Wettlaufer J S, Worster M C, Huppert H E (1997). The phase evolution of young ice. Geophys Res Lett, 24(10): 1251–1254

Zhang J, Steele M (2007). Effect of vertical mixing on the Atlantic Water layer circulation in the Arctic Ocean. J Geophys Res, 112(C4): C04S04